Monthly Notices
of the
ROYAL ASTRONOMICAL SOCIETY

MNRAS **466,** 4888–4903 (2017)
Advance Access publication 2017 January 9

doi:10.1093/mnras/stw3382

The cosmic assembly of stellar haloes in massive early-type Galaxies

Fernando Buitrago,[1,2,3★] Ignacio Trujillo,[4,5] Emma Curtis-Lake,[1,6] Mireia Montes,[7] Andrew P. Cooper,[8] Victoria A. Bruce,[1] Pablo G. Pérez-González[9] and Michele Cirasuolo[10]

[1]*SUPA†, Institute for Astronomy, University of Edinburgh, Royal Observatory, Edinburgh EH9 3HJ, UK*
[2]*Instituto de Astrofísica e Ciências do Espaço, Universidade de Lisboa, OAL, Tapada da Ajuda, P-1349-018 Lisbon, Portugal*
[3]*Departamento de Física, Faculdade de Ciências, Universidade de Lisboa, Edifício C8, Campo Grande, P-1749-016 Lisbon, Portugal*
[4]*Instituto de Astrofísica de Canarias, Vía Láctea s\n, E-38200 La Laguna, Tenerife, Spain*
[5]*Departamento de Astrofísica, Universidad de La Laguna, E-38205 La Laguna, Tenerife, Spain*
[6]*Sorbonne Universités, UPMC-CNRS, UMR7095, Institut d'Astrophysique de Paris, F-75014 Paris, France*
[7]*Department of Astronomy, Yale University, New Haven, CT 06511, USA*
[8]*Institute for Computational Cosmology, DH1 3LE Durham, UK*
[9]*Departamento de Astrofísica, Facultad de CC. Físicas, Universidad Complutense de Madrid, E-28040 Madrid, Spain*
[10]*European Southern Observatory Karl-Schwarzschild-Strasse 2, D-85748 Garching bei Muenchen, Germany*

Accepted 2016 December 30. Received 2016 December 19; in original form 2016 February 4

ABSTRACT

Using the exquisite depth of the *Hubble Ultra Deep Field* (HUDF12 programme) data set, we explore the ongoing assembly of the outermost regions of the most massive galaxies ($M_{stellar} \geq 5\times 10^{10}$ $M_{\odot}$) at $z \leq 1$. The outskirts of massive objects, particularly early-type Galaxies (ETGs), are expected to suffer a dramatic transformation across cosmic time due to continuous accretion of small galaxies. HUDF imaging allows us to study this process at intermediate redshifts in six massive galaxies, exploring the individual surface brightness profiles out to ∼25 effective radii. We find that 5–20 per cent of the total stellar mass for the galaxies in our sample is contained within $10 < R < 50$ kpc. These values are in close agreement with numerical simulations, and higher than those reported for local late-type galaxies ($\lesssim$5 per cent). The fraction of stellar mass stored in the outer envelopes/haloes of massive ETGs increases with decreasing redshift, being 28.7 per cent at $<z>=0.1$, 15.1 per cent at $<z>=0.65$ and 3.5 per cent at $<z>=2$. The fraction of mass in diffuse features linked with ongoing minor merger events is >1–2 per cent, very similar to predictions based on observed close pair counts. Therefore, the results for our small albeit meaningful sample suggest that the size and mass growth of the most massive galaxies have been solely driven by minor and major merging from $z = 1$ to today.

Key words: galaxies: elliptical and lenticular, cD – galaxies: evolution – galaxies: haloes – galaxies: high-redshift – galaxies: structure.

1 INTRODUCTION

There is ample evidence that the most Massive Galaxies (MGs) of the Universe have grown dramatically in size since $z = 3$ (Daddi et al. 2005; Trujillo et al. 2006a,b; Toft et al. 2007; Buitrago et al. 2008; Cimatti et al. 2008; Damjanov et al. 2009; van Dokkum et al. 2010; Cassata et al. 2011; Bell et al. 2012; Bruce et al. 2012; Huertas-Company et al. 2013, to name but a few). Early-type Galaxies (ETGs) – selected by their morphological classification, or through a proxy like colours or quiescent star formation – are those that display the most extreme evolution (with sizes ∼5 times smaller on average, at a given stellar mass, than their local Universe counterparts; Trujillo et al. 2007; Buitrago et al. 2008; van der Wel et al. 2014).

Theoretically, MGs are predicted to undergo a two-phase formation process, whereby there is a initial very rapid and dissipative gas collapse at high-z where most of the in situ stars originate (Khochfar & Silk 2006; Oser et al. 2010; Ceverino et al. 2015; Zolotov et al. 2015; Wellons et al. 2016, see observations in Ricciardelli et al. 2010; Barro et al. 2013; Huang et al. 2013; Williams et al. 2014 as well). The next stage must be a combination of major and minor mergers (Bezanson et al. 2009; Hopkins et al. 2009; Ferreras et al. 2014; Xie et al. 2015), as these processes best reproduce the observed tight scatter in the size–mass relation of MGs, and can

★ E-mail: fbuitrago@oal.ul.pt
† Scottish Universities Physics Alliance.

account for the only mild mass increase in these systems from high redshift to the present day. In this context, some growth is also expected from residual star formation (Pérez-González et al. 2008b; Fumagalli et al. 2014). As a consequence, galaxies progressively build up their outer parts (aka galactic outskirts or outer stellar envelopes) and thus grow in an inside–out fashion (van Dokkum et al. 2010; Trujillo, Ferreras & de La Rosa 2011; Buitrago et al. 2013).

Many observational problems prevent us from directly testing the aforementioned scenario. First, the outskirts of galaxies are intrinsically the faintest parts of these systems. Secondly, surface brightness dimming rises very steeply by $(1 + z)^3$ (see Giavalisco et al. 1996; Ribeiro et al. 2016). Therefore, if these studies are extremely challenging in the local Universe, conducting them at high redshift has been regarded as unfeasible.

Various techniques have been applied in order to overcome these hurdles in the local Universe and to extract the information enclosed in the outer regions of MGs. These include stacking (Zibetti, White & Brinkmann 2004; Tal & van Dokkum 2011; La Barbera et al. 2012; D'Souza et al. 2014), deep photometric studies (Zibetti & Ferguson 2004; Atkinson, Abraham & Ferguson 2013; van Dokkum, Abraham & Merritt 2014; Duc et al. 2015; Trujillo & Fliri 2016), very deep spectroscopic analyses (Coccato, Gerhard & Arnaboldi 2010) or stellar counts (Crnojević et al. 2013; Rejkuba et al. 2014). In doing so, we have learned that ∼70 per cent of the nearby massive ETGs show features indicative of mergers or the tidal disruption of less massive companions (van Dokkum 2005; Tal et al. 2009; Kaviraj 2010). The observed features, such as shells or tidal tails, are red, smooth and extended (sometimes > 50 kpc). This has led to an overall consensus that these galaxies are assembled via mergers involving gas-poor and bulge-dominated systems.

The new observations of the *Hubble Ultra Deep Field* (HUDF), in particular the HUDF12 programme (Ellis et al. 2013; Koekemoer et al. 2013), have opened up the possibility of exploring galaxies to an unprecedented level of detail (5σ limiting magnitude ∼30 AB mag). The extraordinary depth and resolution of these observations, combined with the fact that HUDF12 is the only HUDF programme that preserves the galaxy extended envelopes/haloes, enable us to study galaxy surface brightness profiles down to 31 mag arcsec^{-2} or 25 effective radii (r_e) for the galaxies in our sample, sometimes reaching ∼100 kpc in galactocentric distance.

In this paper, we perform an investigation on the nature of the galaxy outskirts at large galactocentric distances in these ETGs, trying to understand their observables (e.g. percentage of light and mass with respect to the central parts, colours, mass profiles), focusing our study on constraining the mass assembly of MGs, giving the first, direct measurement of the mass growth by ongoing mergers.

The structure of the paper is as follows. Sections 2–4 present the data, the sample and the analysis, respectively. Section 5 shows the several tests we carried out for describing the stellar haloes in our sample of MGs, and finally, Section 6 delivers our summary and conclusions. Hereafter, we adopt a cosmology with $\Omega_m = 0.3$, $\Omega_\Lambda = 0.7$ and $H_0 = 70$ km s^{-1} Mpc^{-1}. We use a Chabrier (2003) initial mass function (IMF), unless otherwise stated. Magnitudes are provided in the AB system (Oke & Gunn 1983).

2 THE DATA

We analysed the deepest ever *Hubble Space Telescope* (*HST*) observations, the HUDF (RA = 03:32:39.0, Dec. = − 27:47:29.1, J2000). In order to detect extended stellar haloes around intermediate-redshift galaxies, the best near-infrared (NIR) data available was provided by the HUDF12[1] programme (Ellis et al. 2013; Koekemoer et al. 2013). This survey combines the images from the HUDF09 programme (Bouwens et al. 2012, and references therein) with a new 128-orbit campaign (*HST* Program ID 12498, PI.: Ellis and McLure). This translates into an outstanding improvement of the previous data set, by enhancing the exposure times (sometimes even quadrupling them, as for the F105W filter) and adding new imaging in the F140W filter. Additionally, and key for our purposes, HUDF12 is unique as its HUDF data reduction preserves the faint wings of extended sources. Finally, in order to obtain the largest multiwavelength *HST* coverage, we also make use of the optical ACS observations[2] over the same area (Beckwith et al. 2006). Therefore, we have investigated the area (4.7 arcmin^2) where WFC3 and ACS observations overlap. We list the photometric bands, total exposure times and zero-points in Table 1.

We also need to understand whether the level of background fluctuations in these data enables us to characterize very faint surface brightness features. We conducted a thorough characterization of each science image by placing 25 000 random square 1×1 arcsec apertures in empty sky patches, inferring a surface brightness limit of ≥31 mag arcsec^{-2} (only slightly brighter for Z band) at a 3σ level over the background fluctuations in 10×10 arcsec boxes. The WFC3/IR images have passed multiple checks regarding their sky background properties, especially about persistence and large-scale flat-field variations. After the applied residual corrections, the sky is flat to within ∼1–2 per cent of mean sky level, translating into uniform limiting depths (≤0.03 mag) throughout the images. On the other hand, as it has been already indicated, the ACS programme targeting the HUDF is prior to the HUDF12 campaign, which is actually an asset to minimize the charge transfer efficiency degradation caused by radiation damage. It is to note that careful flat-fielding and treatment of the scattered light was undertaken, as described at length in the section 3.1 in Beckwith et al. (2006). The final residual flux is also <2 per cent of the sky level.

3 THE SAMPLE

The criteria for our galaxy selection are the following: ETG visual morphology, $M_{stellar} > 5\times 10^{10}$ M$_\odot$ and $z_{spec} \lesssim 1$ (to avoid severe cosmological dimming effects). We find six objects satisfying these criteria. These galaxies are also the most massive within the HUDF up to this redshift limit. Our galaxy sample was first identified by means of the Rainbow data base[3] (Pérez-González et al. 2008a; Barro et al. 2011a,b).

Spectroscopic redshifts are available for our whole sample (Croom et al. 2001; Le Fèvre et al. 2005; Vanzella et al. 2005; Ravikumar et al. 2007). In order to be self-consistent and to use the information in the HUDF images, instead of using the Rainbow mass estimates, we performed Spectral Energy Distribution (SED) fitting using the Le Phare photometric redshift code (Arnouts et al. 1999; Ilbert et al. 2006) to obtain stellar masses for each object based on the total fluxes derived from the four Sérsic component fits plus residuals (see Section 4.1). A range of short duration tau models (30, 70, 100, 300 Myr e-folding time) and a burst model were included in the template set. The models were produced using Bruzual & Charlot (2003, BC03) at solar metallicity with a Chabrier (2003) IMF. The fitted ages were required to be younger than the age

[1] http://archive.stsci.edu/pub/hlsp/hudf12/
[2] http://archive.stsci.edu/pub/hlsp/udf/acs-wfc/
[3] https://rainbowx.fis.ucm.es/

Table 1. List of filters.

Instrument	Filter	Exposure time (s)	Zero-points (mag)	PSF FWHM (arcsec)	Pixel scale (arcsec pix^{-1})
ACS	F435W	134 880	25.673	0.080	0.03
ACS	F606W	135 320	26.486	0.073	0.03
ACS	F775W	347 110	25.654	0.080	0.03
ACS	F850LP	346 620	24.862	0.085	0.03
WFC3	F105W	333 877	26.269	0.181	0.06
WFC3	F125W	193 307	26.230	0.185	0.06
WFC3	F140W	82 676	26.452	0.187	0.06
WFC3	F160W	317 944	25.946	0.190	0.06

Table 2. List of galaxies.

Galaxy name	RA (J2000)	Dec. (J2000)	z_{spec}	$Mass_{Chabrier}$ [log($M_\odot$)]	$Mass_{Salpeter}$ [log($M_\odot$)]	$r_{e,\,H band}$ (arcsec)	$r_{e,\,circ,\,H band}$ (kpc)	Axis ratio b/a	Pos. angle (°)
HUDF-1	53.161 61	−27.780 30	0.619	$10.42^{+0.03}_{-0.03}$	10.65	0.34 ± 0.02	1.70 ± 0.15	0.54 ± 0.01	33.44±0.10
HUDF-2	53.172 53	−27.788 17	0.622	$10.81^{+0.16}_{-0.03}$	11.04	0.63 ± 0.06	3.06 ± 0.35	0.52 ± 0.01	−47.07 ±0.03
HUDF-3	53.148 93	−27.799 76	0.664	$10.90^{+0.05}_{-0.01}$	11.13	0.42 ± 0.03	2.66 ± 0.21	0.81 ± 0.01	−26.77 ±0.10
HUDF-4	53.163 41	−27.799 62	0.665	$10.81^{+0.07}_{-0.03}$	11.04	0.25 ± 0.02	1.59 ± 0.11	0.83 ± 0.01	22.04±0.08
HUDF-5	53.155 43	−27.791 56	0.667	$11.19^{+0.09}_{-0.05}$	11.42	0.63 ± 0.05	4.16 ± 0.34	0.90 ± 0.01	75.18±0.07
HUDF-6	53.154 91	−27.768 95	1.096	$11.43^{+0.00}_{-0.03}$	11.66	0.68 ± 0.05	4.54 ± 0.32	0.68 ± 0.01	68.52±0.04

of the Universe at the redshift of the source, and no dust extinction was allowed in the fitting, because it is expected to be of negligible importance for massive ETGs. The outcomes for our galaxy sample are listed in Table 2.

We also supplement the table with the masses changed to a Salpeter (1955) IMF (+0.23 dex, as in Cimatti et al. 2008) due to increasing evidence for a more bottom-heavy IMF for MGs (Ferré-Mateu, Vazdekis & de la Rosa 2013; La Barbera et al. 2013; Martín-Navarro et al. 2015). We stress that, according masses derived with a Chabrier IMF, HUDF-1 falls below our mass cut. However, given that the mass derived with a Salpeter IMF does meet our criteria, we chose to keep this object in our sample as it is among the most massive objects in HUDF at $z < 1$.

A montage with the galaxies in our sample is shown in Fig. 1. The ubiquity of morphological low surface brightness features displayed by these galaxies is noteworthy (like the shells in HUDF-3 or the fan of stars in HUDF-5). In addition, a large number of minor objects surrounding the MGs are present. It is beyond the scope of this paper to identify them as galactic satellites, but we would expect to see a large number of satellites if minor merging is significantly contributing to the evolution of MGs (Bluck et al. 2012; López-Sanjuan et al. 2012; Mármol-Queraltó et al. 2012, 2013; Newman et al. 2012; Ferreras et al. 2014; Ruiz, Trujillo & Mármol-Queraltó 2015).

4 THE ANALYSIS

The survey images were carefully reduced and sky-subtracted (Koekemoer et al. 2013). We created 400 kpc wide postage stamps to explore the light distribution around the galaxies in the eight filters available. We masked the neighbouring objects using SExtractor-based (Bertin & Arnouts 1996) optical and NIR masks, which were later visually inspected and modified to remove any spurious light contribution. The final depictions of our masks upon the galaxy images are shown in Figs 2 and 3. The displayed images are the coaddition of all NIR and optical bands and they have also been smoothed by a 2-arcsec standard deviation Gaussian kernel. These choices have been taken in order to highlight the lowest signal-to-noise features in the images. It is also fair to say that, despite the generous masking that has been applied, it is impossible to get rid of every single source of contamination. Nevertheless, after this careful effort, all the MGs steadily decrease their surface brightness profiles down to the detection limits (golden ellipses).

We also require very accurate local sky subtraction as any residual background hampers our efforts for exploiting the extraordinary depth of our imaging. This aspect is particularly relevant if one is to sample very faint surface brightness features, and we proceeded as in Trujillo & Bakos (2013). We determined that the sky noise was dominant at galactocentric distances higher than 120 kpc for all galaxies. Therefore, we estimated the sky level in each image at a radial distance of $140 < R < 160$ kpc and subtracted that value. This meticulous analysis enables us to detect galaxy light down to 31 mag arcsec^{-2} (3σ in 10×10 arcsec boxes), consistent with the limiting magnitude determinations in McLure et al. (2013).

For sampling the galaxy surface brightness profiles from our galaxy sample, we created concentric elliptical apertures from the galaxy centre, 0.5 kpc wide in the inner 2 kpc, and 2 kpc wide at greater distances. We fixed the axis ratio and position angle of these elliptical apertures to the H-band single Sérsic outputs (see Subsection 4.1) in order to sample consistently the surface brightness profiles for all filters. The H-band filter is chosen because it is the reddest, and as such, it is the most representative of the total stellar component. In those annuli, we estimated the galaxy flux by the 3σ clipped mean of the pixel values on those apertures, and then we apply the formula

$$\Sigma\left[\mathrm{mag/arcsec^2}\right] = -2.5\log\left(F_{\mathrm{annulus}}\right) + zp + 5\log\left(S_{\mathrm{pix}}\right), \qquad (1)$$

where Σ is the galaxy's surface brightness, F_{annulus} is the average flux per pixel within the annulus, zp stands for each image zero-point and S_{pix} is the pixel scale (0.06 arcsec pix^{-1} for WFC3 and 0.03 arcsec pix^{-1} for ACS). The only object that was not totally explored using this method is HUDF-3, whose WFC3 images do not cover the whole galaxy (see Fig. 1).

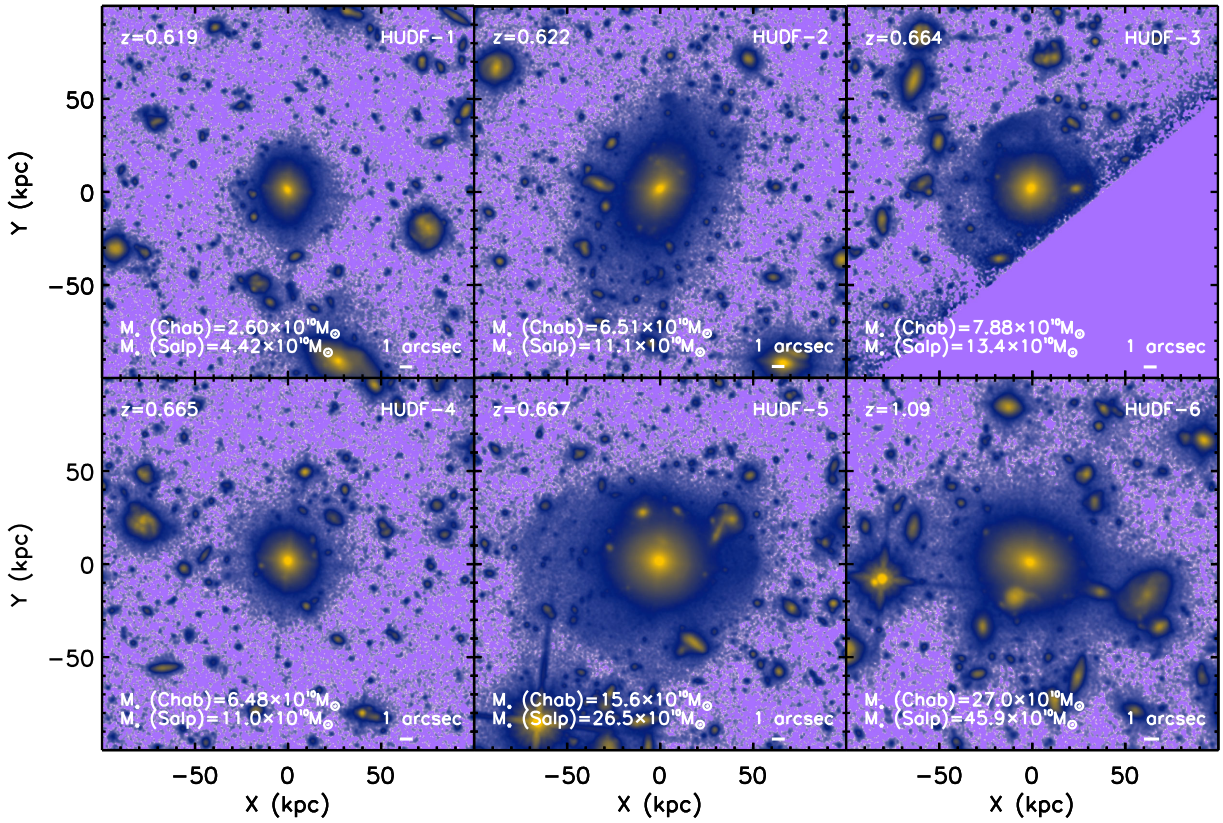

Figure 1. Montage with the HUDF12 WFC3 images for our sample of massive ETGs, also showing their spectroscopic redshifts and photometric masses. These are the stacked *HST* NIR images, and the colour palette ranges from 18 to 30 mag arcsec^2. The superb WFC3 resolution (approximately 0.18 arcsec, $\sim$1.25 kpc at $<z>=0.65$, the median redshift of our observations) allow us to see the huge stellar envelopes for these objects, apart from broad fans of stars or shells (for HUDF-3 and HUDF-5) and other asymmetries. It is also striking the presence of so many potential satellites, which may contribute to the size increase of the massive objects via minor merging.

4.1 Surface brightness fitting and the impact of the PSF

The Point Spread Function (PSF) of the images not only sets the angular resolution of our observations but also determines how the galaxy light is scattered (see Sandin 2014, 2015 for a recent analysis). Hence, correcting the observed surface brightness profiles by the PSF distortion is essential to retrieve accurate 2D surface brightness maps and structural parameters. To that end, we have fitted using GALFIT (Peng et al. 2010), from 1 to 4 Sérsic functions to all the images of the galaxies within our sample. The reason behind our multicomponent fitting is to ensure that we are describing the 2D distribution of each galaxy's light to the greatest level of detail permitted by our privileged photometry, avoiding any possible overmodelling ($\chi^2_\nu < 1$). By so doing, it is important to realize that we cannot give any physical interpretation to the different Sérsic function fits to the galaxy surface brightness profiles in ETGs, as done by other studies focused on late-type galaxies (Zibetti & Ferguson 2004; Trujillo & Bakos 2013), without the addition of kinematic information (Falcón-Barroso et al. 2006; Krajnović et al. 2008, 2013).

The Sérsic functions are axisymmetric, and as such, it is impossible (unless you perform an ad hoc fit in a particular set of pixels of your image) to model any non-symmetric substructure in the galaxy's surface brightness profiles. We thus selected as the best galaxy model the 4-Sérsic deconvolution adding the residuals of the fit – as done in Szomoru, Franx & van Dokkum (2012), hereafter 'a la Szomoru' method – trying to capture any possible feature not represented by the symmetric Sérsic functions. Contrary to this 'a la Szomoru' method, we masked the central 10 pixels when performing the residual addition as these central pixels have some artificial noise owing to the exact positioning of the PSF peak. Please see Appendix A for a comparison of these 'a la Szomoru' surface brightness profiles with the rest of the fits, as well as the observational galaxy profiles.

It is to note that neighbour galaxies have been masked but not subtracted in our GALFIT fits, and thus a certain level of light contamination is expected. We ensure that in all cases (except HUDF-6), none of the five brightest objects in each galaxy stamp is within our limit for the surface brightness determination. For our exception, HUDF-6 images show a companion star at $\sim$10 arcsec from the galaxy's centre. The difference between fitting or not (using of course a PSF model) this star for the galaxy total flux is <0.02 per cent, and thus negligible.

Our PSF choice must not only be accurate but very extended as well, in order to prevent any red spurious excess at large radii mimicking the light contribution of a stellar halo (the so-called red halo problem, e.g. Zibetti et al. 2004; Zibetti & Ferguson 2004; Zackrisson et al. 2006; de Jong 2008). In theory, we should go as far as 1.5 times the full galaxy size (Sandin 2014, 2015; Trujillo & Fliri 2016). TINY TIM (Krist 1995) is the only way to build such extended *HST* PSFs. Therefore, we created our Tiny Tim simulated stars by assuming they should extend up to the equivalent size of 200×200 kpc at the median redshift ($<z>=0.65$) of our galaxy sample. This translates into PSF sizes of 500×500 pixels for WFC3

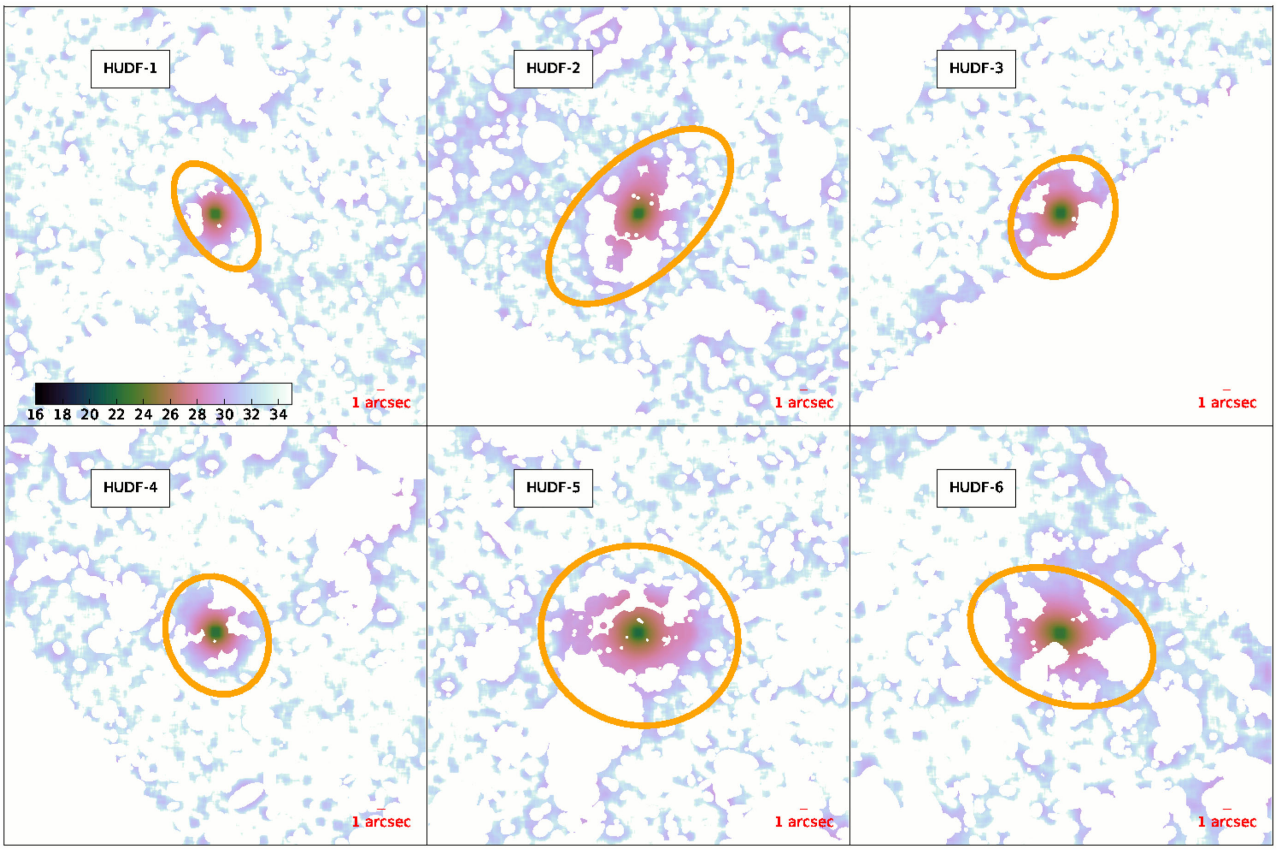

Figure 2. Coaddition of all NIR WFC3 images. The resulting image has been smoothed by convolving a 2-arcsec standard deviation Gaussian kernel and then our NIR mask of the galaxy neighbours has been overplotted. The whole process is done in order to highlight the lowest signal-to-noise features in the image. The colourbar displays the surface brightness in units of mag arcsec^{-2}. The golden ellipse shows the extent of our surface brightness analysis in the *H* band (reddest band in the NIR).

and 1000×1000 pixels for ACS. However, for ACS images, Tiny Tim cannot retrieve models spanning such large distances, and thus we content ourselves with the maximum extent possible for this camera. However, this fact has very little (if any) impact in our analysis because of the very small sizes of our passive galaxy sample in the bluest bands.

We further improved the PSF produced by Tiny Tim in each band by replacing the core with that of an isolated non-saturated star at RA = 03:32:38.01, Dec.=−27:47:41.67 (J2000). This mitigates the effect shown by Bruce et al. (2012), whereby Tiny Tim underpredicts the PSF flux at distances greater than 0.5 arcsec. We also rotated these hybrid stars in order to match the position of the stellar spikes in HUDF science image. The chosen star's spectral type is K4–K5 star (Pirzkal et al. 2005), which is optimal for studying ETGs as the light from both the star and the galaxies is scattered similarly in broad-band filters (La Barbera et al. 2012).

After these considerations on our PSF model, we checked about the existence of the 'red halo' problem in our sample. The test we performed is to be found in Fig. 4. We compare there our observed surface brightness profiles, the 'a la Szomoru' profiles and the PSF profiles (scaling them up to match the peak in the galaxies' surface brightness profiles). These are space observations (small PSF FWHM), and as such there is not so much difference between the convolved and unconvolved + residuals profiles. It is also reassuring that the outer parts of the galaxies do not decrease in a similar way as the PSF profiles, and thus limiting the impact of the 'red halo' problem. What we find is that there is an exponential decay for HUDF-2 in the NIR bands between 3 and 8 arcsec, indicating the presence of an inner disc. We will further discuss about it in Section 5.4. Finally, we did another similar exercise comparing star and galaxy profiles, but normalizing this time the PSFs to the total galaxy fluxes. We obtained similar conclusions.

5 RESULTS

We show our observed surface brightness profiles in Fig. 5. It is worth noting that the various galaxies in our sample show emission extending to different galactocentric distances and that none of them have signs of abrupt truncation even at the faint levels explored. Every galaxy is more extended and more luminous in the redder bands as expected for passive ETGs. For some of the objects, we reach 10–12 arcsec in the *H* band, which is comparable to local Universe very deep observations (Kormendy et al. 2009; Tal & van Dokkum 2011) but this time at a median redshift $<z> = 0.65$, where the cosmological dimming make all galactic features ∼2 mag arcsec^{-2} fainter.

5.1 Sloan equivalent filters and colours

We have calculated Sloan bands equivalent rest-frame surface brightness profiles for the six galaxies in our sample (Fig. 6) for determining colours and masses at each step in galactocentric distance. They were constructed from both the observed and

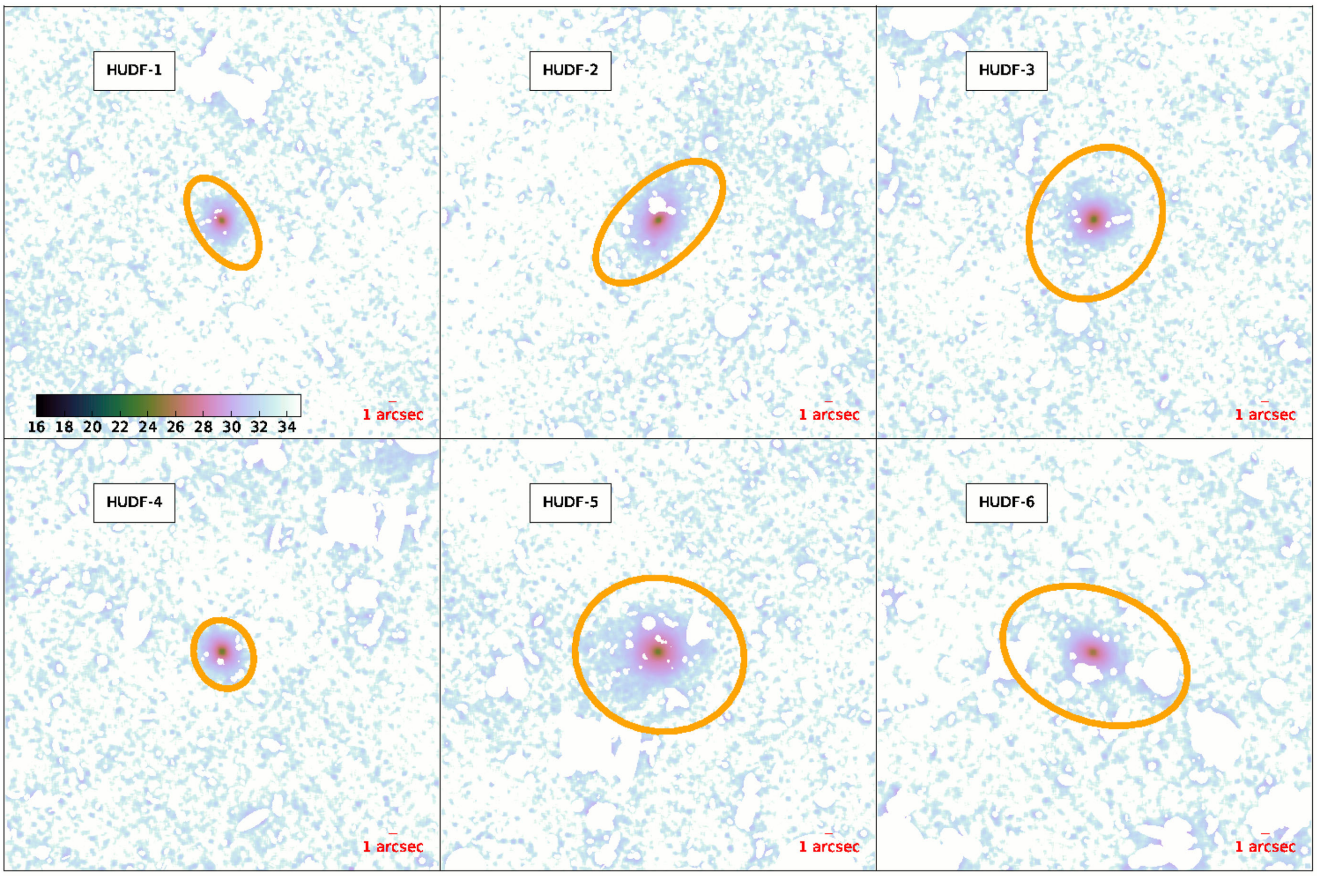

Figure 3. Coaddition of all optical ACS images. The resulting image has been smoothed by convolving a 2-arcsec standard deviation Gaussian kernel and then our optical mask of the galaxy neighbours has been overplotted. The whole process is done in order to highlight the lowest signal-to-noise features in the image. The colourbar displays the surface brightness in units of mag arcsec^{-2}. The golden ellipse shows the extent of our surface brightness analysis in the Z band (reddest band in the optical).

the model+residual 'a la Szomoru' profiles by linearly interpolating the *HST* filters and then correcting the surface brightness by cosmological dimming (as done before in Trujillo & Bakos 2013). It is noticeable that the PSF effects are more pronounced for the central parts, where the galaxy flux is more concentrated, and for the redder filters, as the WFC3 PSF is broader than the ACS one. As expected, correcting for the PSF produces brighter galaxy cores and slightly fainter profiles at intermediate galactocentric distances, while at larger distances (>30 kpc) the effect is almost negligible. For the galaxies HUDF-2, HUDF-3 and HUDF-5, a number of quite distinctive surface brightness bumps at magnitude ∼25 are visible. They are especially strong for the redder bands. In the latter two cases, the association with recent merger events is evident, looking at the visual morphologies in the NIR bands. For the remaining one, this may be also the case, as it looks very asymmetric in the same photometric bands.

With these profiles, we computed the Sloan filters equivalent $u-g$, $u-r$, $g-r$, $g-z$ and $r-i$ colours in Fig. 7 up to 30 kpc. The inner parts of the colour profiles are uncertain due to the few pixels that enter in our concentric ellipses for the surface brightness calculations. For instance, observing with WFC3 (0.06 arcsec pix^{-1}) a galaxy at $z = 0.65$ (∼7 pix arcsec^{-1}) means that the inner kpc is comprised in a radius of ∼ 2 pixels. After the central kpc, the profiles are rather flat. We choose not to show beyond 30 kpc because of the larger error bars (>0.2 mag) and also upbends in some profiles. The reason behind these odd colours at large galactocentric distances is the aggressive sky subtraction, as the HUDF was optimized to look for high-z galaxies, and therefore, any very extended structure is affected even with our careful data reduction.

5.2 Stellar mass profiles

Fig. 8 shows the circularized stellar mass density profiles for the galaxies in our sample. We calculated them using the prescriptions in Roediger & Courteau (2015) appendix A table 2 for mass-to-light ratios using Sloan colours. Specifically, for the galaxies at $<z>=0.65$, our choice of colour and base profile was $g-z$ and z, and for HUDF-6 we utilized $u-r$ and r. These sets of colours and bands were chosen in order that the blue band is only constructed from the ACS filters and the red band uses only WFC3 information. Consequently, we avoid any PSF mismatching effects that may arise in case one combines photometric data coming from two different cameras. We normalized the total masses by those obtained from the SED fitting. Overplotted are the mass profiles for similar mass ($8\times10^{10} < M_{\rm stellar}$ / M$_\odot$ $< 1.2\times10^{11}$) ETG galaxies (Sérsic index $n > 2.5$) in NYU catalogue (Blanton et al. 2005) at $0.08 < z < 0.12$ (the uncertainties are given as a shaded red region) and the massive and compact galaxies in Szomoru et al. (2012) at $1.75 < z < 2.5$ (with mean $r_{\rm e,\,circ} = 0.98$ kpc and $n = 3.92$). For both our sample and Szomoru et al.'s, we provide the individual and mean profiles, We choose to stop ours at 30 kpc in order not to be

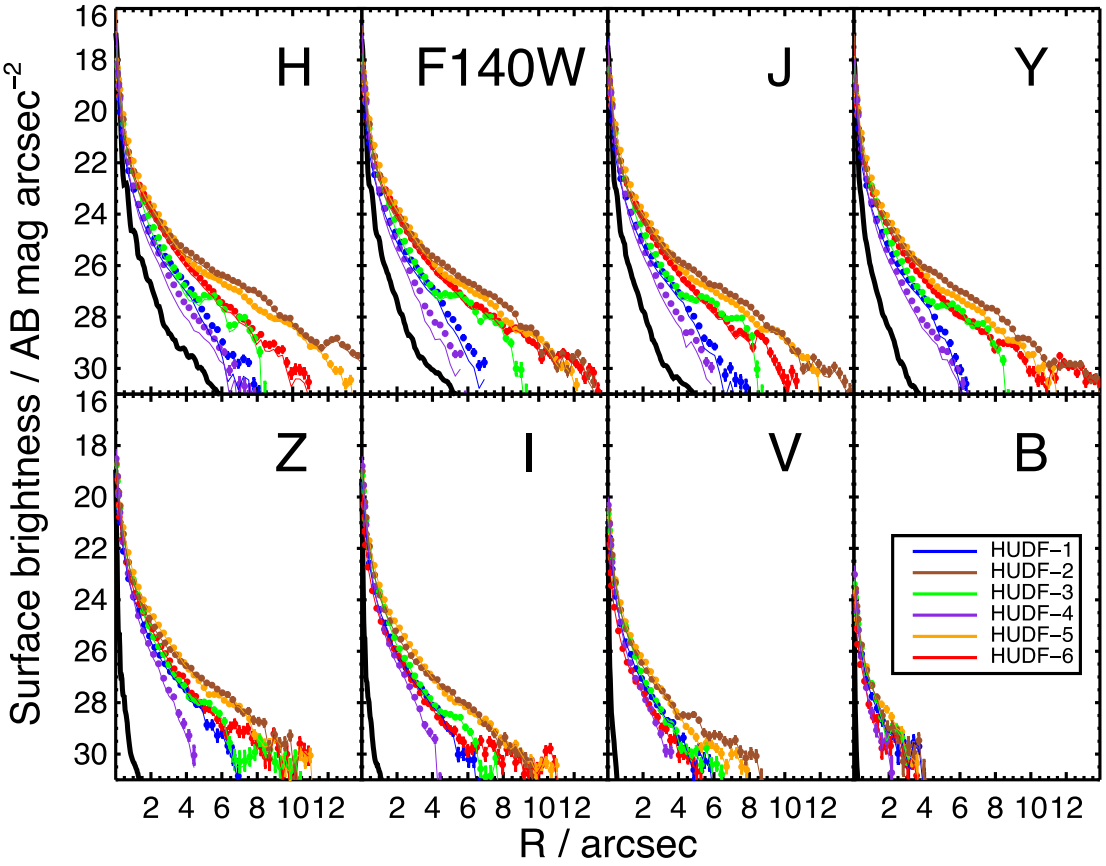

Figure 4. Comparison among the observed galaxy surface brightness profiles (coloured points), the best galaxy surface brightness models ('a la Szomoru': deconvolved profiles + residuals; coloured lines) and the PSF profiles (scaled up to match the galaxy centres; black lines) for each *HST* band. As expected for large ETGs in space observations (small PSF FWHM), the convolved and unconvolved profiles are not very different. Moreover, the outer parts of the galaxies do not decrease their brightness in a similar way than the PSF profiles, limiting any 'red halo' issue in our sample.

affected by any colour uncertainties in our light-to-mass conversions. Our sample of massive HUDF ETGs shows extended stellar haloes not present in the compact high-z galaxies (Bezanson et al. 2009; Cassata et al. 2010; Szomoru et al. 2012; Trujillo et al. 2014), thus showing closer resemblance to the SDSS local counterparts.

In order to parametrize this variation, we have integrated these mass mean profiles between 10 and 50 kpc, where we can compare our results with state-of-the-art simulations (Cooper et al. 2013, see Section 5.3 in this paper). As neither Szomoru's nor our mass profiles extent to that distance, we fit the mean profiles in the two cases to Sérsic functions and extrapolate these functions up to 50 kpc. Then, we integrate these functions between 10 and 50 kpc. The results are remarkable, while 3.5 per cent of the galaxy mass is enclosed at these distances for Szomoru et al.'s case ($<z>=2$), the fraction is 15.1 per cent at $<z>=0.65$ and 28.7 per cent at $<z>=0.1$. Despite the fact that the total stellar mass for the three mean profiles is similar ($\sim 10^{11}$ M$_{\odot}$), the mass profiles of massive ETGs at high-z are intrinsically different than those at lower redshifts.

In Fig. 9, we provide a more in-depth quantification of the amount of light (both for the reddest filter, the H-band and the z-band rest frame which is the band we used to build the mass profiles) contained in the galaxies of our sample using the same elliptical apertures we utilized for deriving the surface brightness profiles. Between 20 per cent and 40 per cent of the light is distributed at distances beyond 10 kpc. The only MG that differs slightly (more light concentrated in the inner parts and less in the outskirts) is the compact HUDF-4. It is not possible to discern any sharp transition between the galaxies' cores and their external parts by either visually inspecting these plots or the mass profiles in Fig. 8.

5.3 Comparison with state-of-the-art simulations

In this subsection, we compare our observational results with the theoretical models of Cooper et al. (2013, hereafter C13). These simulations use a semi-analytic model of galaxy formation (Guo et al. 2011) in combination with a cosmological N-body simulation (Boylan-Kolchin et al. 2009) to predict the surface mass density profiles of ∼1900 galaxies hosted by dark matter haloes of mass 10^{12}–10^{14} M$_{\odot}$.

In simulations, it is possible to distinguish stars that are accreted by galaxies from so-called in situ stars formed directly in their host dark matter haloes. In observations, the various subcomponents of late-type galaxies follow different light distributions, allowing the canonical bulge–disc–halo decomposition (e.g. Trujillo & Bakos 2013). In ETGs, however, both in situ and accreted stars are distributed in spheroidal components that cannot be separated unambiguously by decomposition of their surface brightness profiles. To proceed, we make use of the fact that the C13 models predict that accreted stars have much lower binding energies on average than in situ stars, with the result that essentially all stellar mass beyond a certain galactocentric radius is accreted. The mass obtained by integrating both observed and simulated mass profiles outwards from a sufficiently large radius therefore provides a fair

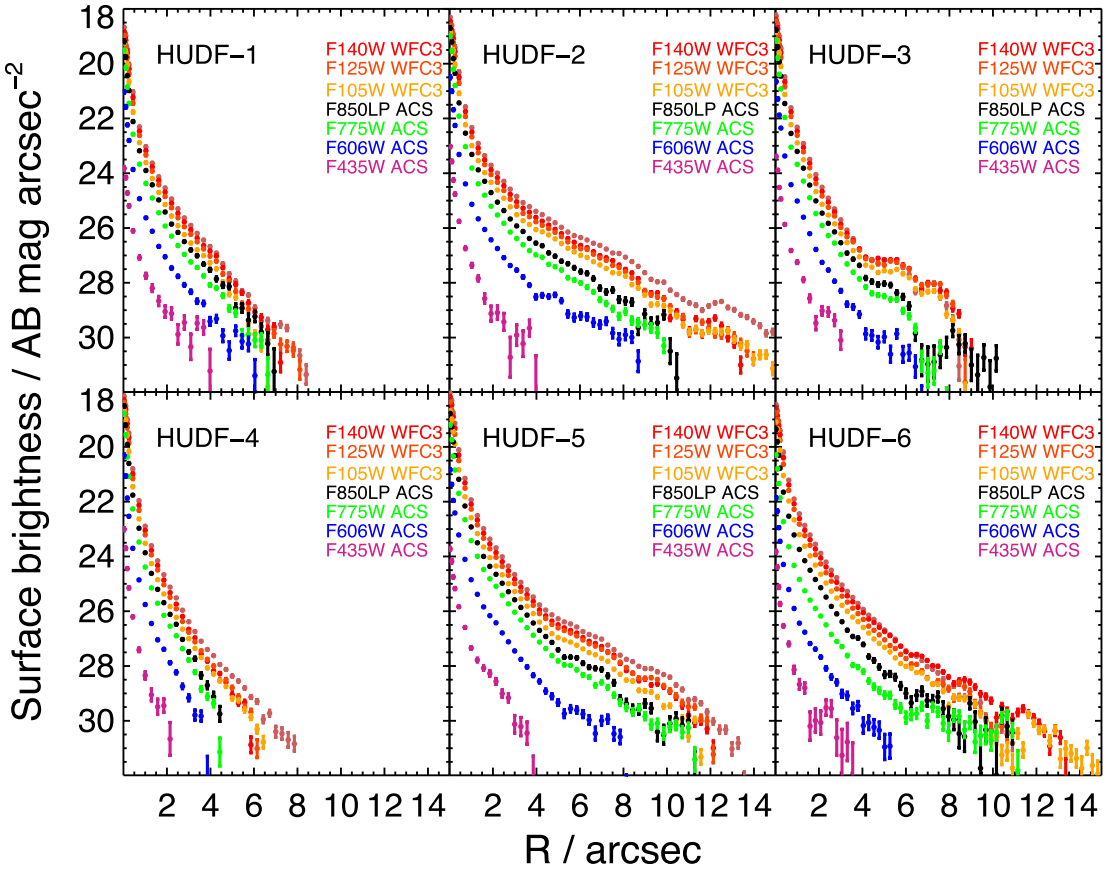

Figure 5. Observed surface brightness profiles measured within each of the *HST* filters available for our ETG sample. Each individual point was calculated in elliptical 2 kpc wide apertures (except for the central four points where 0.5 kpc wide apertures were used), applying a 3σ clipped mean in those annuli, for retrieving the surface brightness values and the associated error bars. For all cases, these massive ETGs are more luminous and extended in the redder bands. The galactocentric distances probed in this study, sometimes more than 100 kpc at $z = 0.6$–1, are comparable with local Universe ETG very deep observations (Kormendy et al. 2009; Tal & van Dokkum 2011).

point of comparison, even though it does not correspond to the total mass of accreted stars in either case.

In the C13 simulations, late and early types are separated by the ratio of bulge-to-total mass predicted by the Guo et al. (2011) model (B/T less or greater than 0.9, respectively). The particle tagging method used by C13 to predict surface brightness profiles introduces an additional free parameter beyond those of the Guo et al. model, $f_{\rm mb}$. This controls the depth in the host dark matter potential at which newly formed 'stars' are inserted into the simulation. For example, a value of $f_{\rm mb} = 1$ per cent means that newly formed stellar populations initially have a binding energy distribution identical to that of the most tightly bound 1 per cent of the dark matter in their host dark matter halo (see C13 for details). C13 explore a range of values for this parameter, which they find to be strongly constrained to a range 1–5 per cent by the observed size–mass relation of galaxies dominated by in situ stars (i.e. discs) at $z = 0$. In practice, the precise choice of $f_{\rm mb}$ makes only a very marginal difference to the results we discuss here (C13; Trujillo & Fliri 2016). Therefore, we report comparisons against the $f_{\rm mb} = 1$ per cent results of C13.

The further from the centre of the galaxy, the lower is the contribution by in situ material to the mass profile. Being conservative, we will start our integration from the typical distance, where high-z MG surface brightness profiles finish (∼10 kpc, see Fig. 8) and hence identify our stellar haloes as the light component previously missed in shallower observations. We stop our calculations at 50 kpc, our previous integration limit. The results for our galaxy sample are plotted in Fig. 10, and their error bars stem from the difference in the mass determinations by using either the Roediger & Courteau (2015) or the Bell et al. (2003) recipes. We also supply the local galaxy mass fraction at $10 < R/{\rm kpc} < 50$ relationships from the C13 simulations for ETGs. This relationship is displayed in red colour, with the 16 and 84 quartiles being the dashed lines. For consistency, we also overplot the extrapolations for the individual massive ETGs in Szomoru et al. (2012) and the mean values for the three samples we are using throughout this paper (namely Szomoru's, HUDF and SDSS).

There is an overall departure of our galaxy sample from the local relation, most probably due to the fact that they are not $z = 0$ galaxies ($<z> = 0.65$ median redshift). In fact, the six MGs in our sample straddle the high-z and low-z data. Combining the location of the $<z> = 2$ data points and Fig. 8, it seems that the HUDF ETGs are advancing towards the upper part of the plot to reach their fiducial $z = 0$ relation. Very interestingly, there is a correlation between the total galaxy mass and fraction of mass in the outer parts for our six galaxies, where they approximately follow the Cooper et al.'s ETG predictions. It is also remarkable, the agreement between Cooper's simulations and the SDSS mean value.

Quantitatively, fig. 8 (left-hand side) in Trujillo & Bakos (2013), fig. 4 in van Dokkum et al. (2014) and fig. 13 in Trujillo &

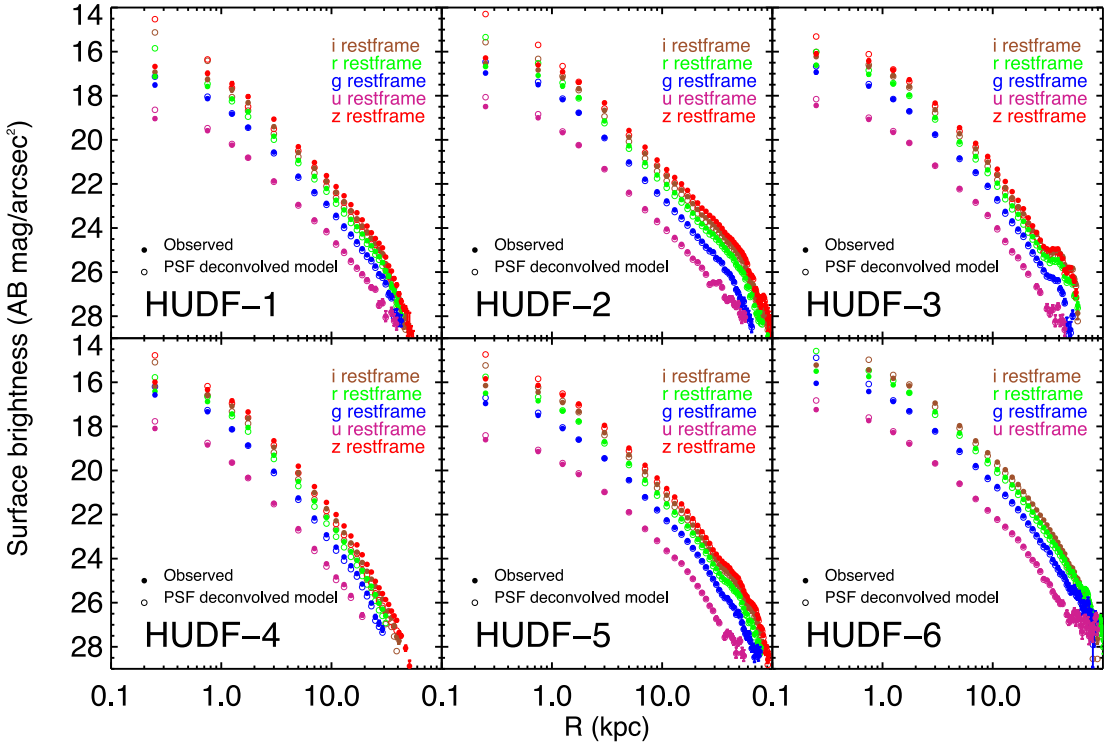

Figure 6. The *u*-, *g*-, *r*-, *i*- and *z*-band Sloan filters equivalent rest-frame surface brightness profiles for the six galaxies in our sample. They were created by linearly interpolating the *HST* filters, both for the observed and the model+residual 'a la Szomoru' profiles, and then correcting the surface brightness by cosmological dimming. Note that, for HUDF-6, *z* band is not covered due to its redshift ($z \sim 1.1$). It is clear that the PSF effect scattering the light coming from these objects is more pronounced for the inner galaxy parts. It is also interesting checking that HUDF-2, HUDF-3 and HUDF-5 have bumps at rest-frame surface brightness 25–26 mag arcsec^{-2}, and they are specially strong in the redder bands. By joining this information with their visual appearance, we associate these features to recent merging events.

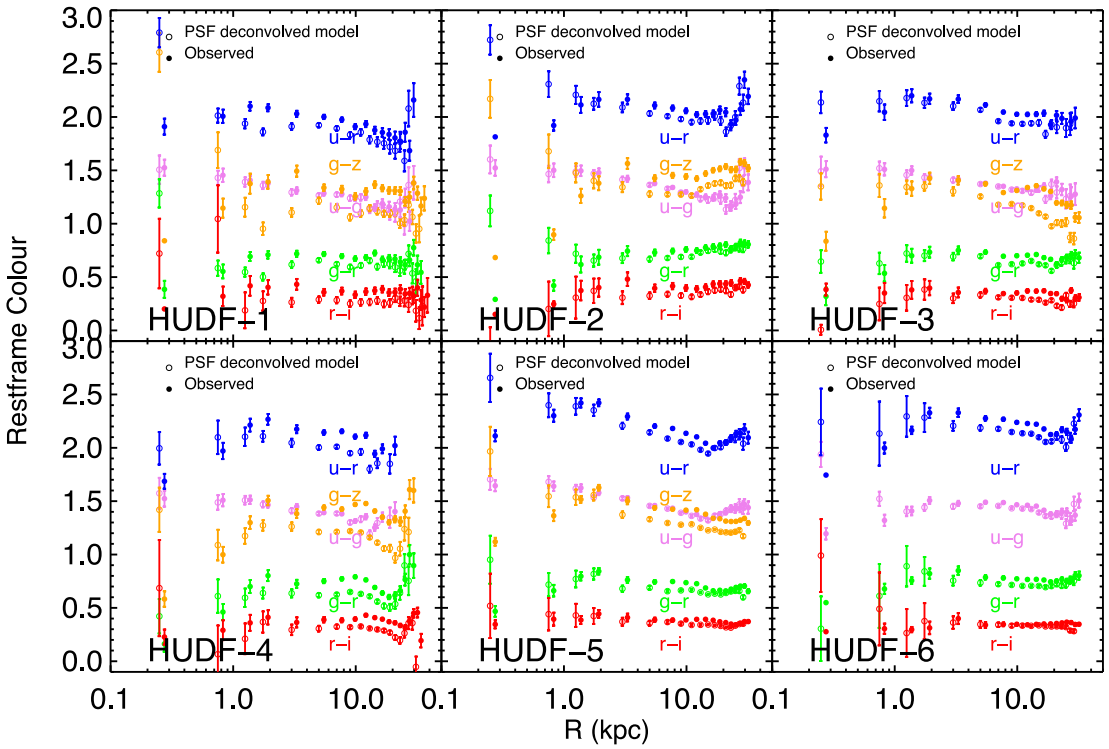

Figure 7. The $u-g$, $u-r$, $g-r$, $g-z$ and $r-i$ Sloan filters equivalent rest-frame colour profiles for the six galaxies in our sample. Both observational and model+residual 'a la Szomoru' profiles area plotted (with a slight shift in the *x*-axis for a better reading), along with their errors up to the limit of 30 kpc.

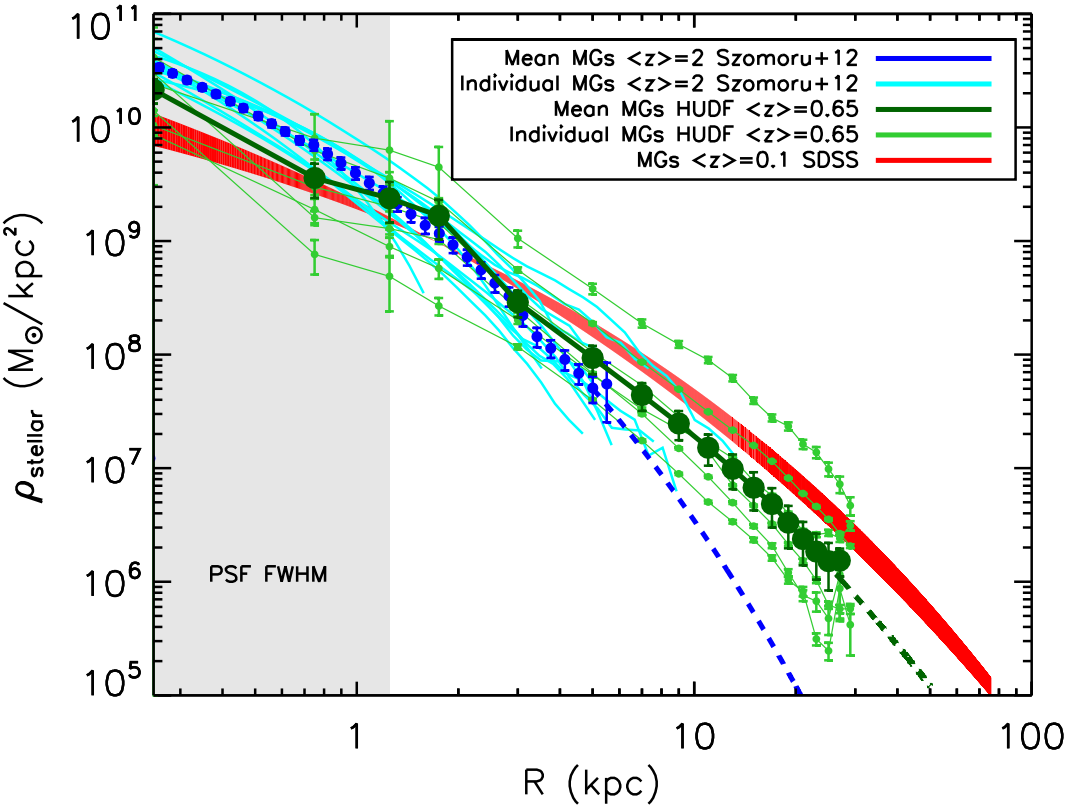

Figure 8. The circularized stellar mass density profiles for the MGs in our sample, comparing them with similar mass SDSS ETGs and the massive compact galaxies in Szomoru et al. (2012). Individual mass profiles are shown in light colours, while the mean profiles are in dark colours (and their extrapolations are the dashed lines). HUDF MGs show an excess of mass in their outer parts, opposite to what could be seen for the high-z sample, and closer what was found for local massive ETGs. This evidence points to the progressive building up of stellar haloes as the link between the two other populations.

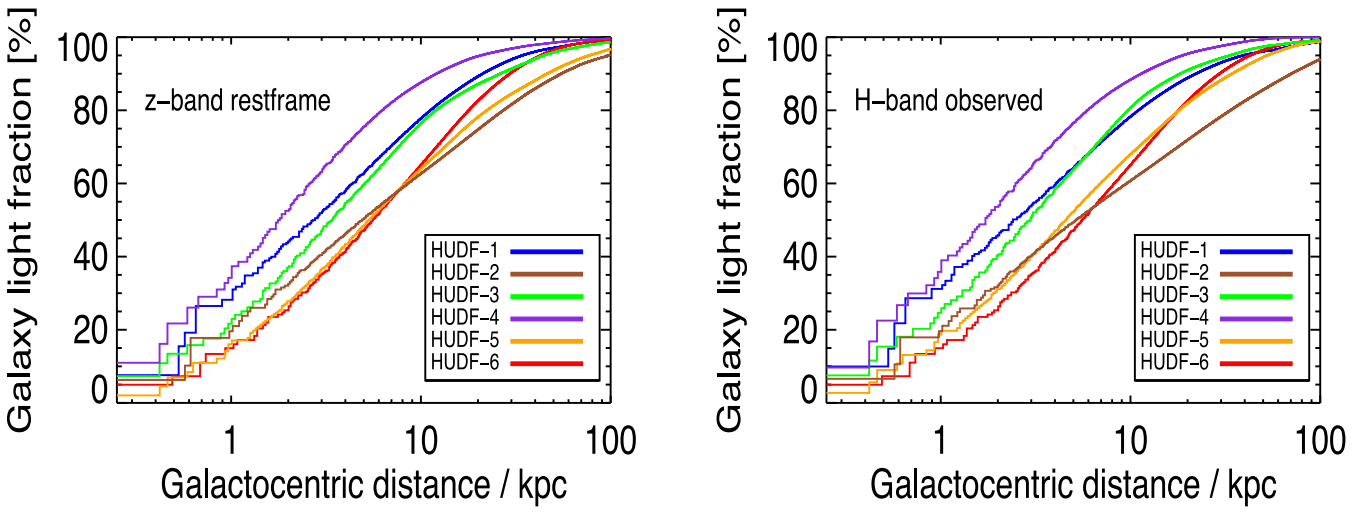

Figure 9. Cumulative light fractions for our inferred z-band rest frame (the base for our mass profiles) and the reddest observed band (H). Except for HUDF-4, the most compact galaxy, the rest of the MGs store between 20 and 40 per cent of their light at galactocentric distances greater than 10 kpc.

Fliri (2016) show that the haloes of $M_{\rm stellar}$ $\sim$$10^{10}$–$10^{11}$ $M_{\odot}$ late-type galaxies constitute at most 5 per cent of their total light at $z = 0$. Our small but unique sample shows that the stellar mass in massive ETG stellar haloes is larger of the order of 5–20 per cent (and yet not at $z = 0$, but at $z \sim 0.65$). This contrast between galaxy types must be investigated further (see for instance D'Souza et al. 2014), but makes sense from a Λ cold dark matter (ΛCDM) perspective, where the histories of ETGs should be more merger-dominated than for discy galaxies (Cole et al. 2000; Croton et al. 2006; Purcell, Bullock & Zentner 2007; Ruiz et al. 2015), and also because ETGs do not have a prominent disc storing a significant fraction of the galaxy's baryons.

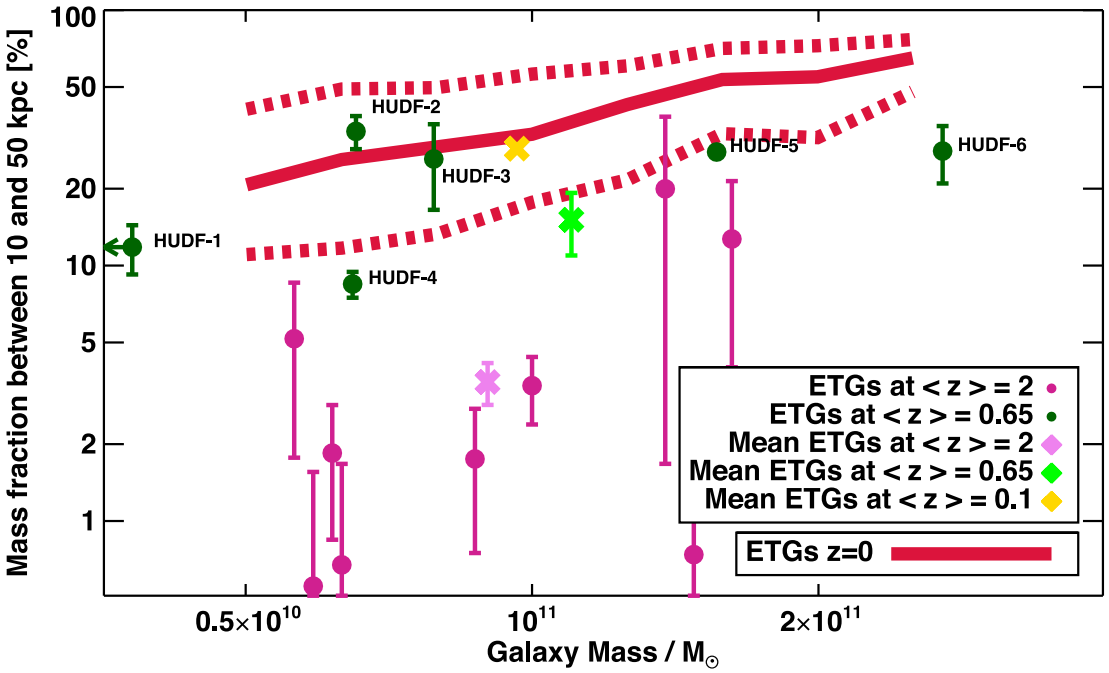

Figure 10. Fraction of the galaxy stellar mass between 10 and 50 kpc versus the total stellar mass for our sample of six ETGs (the green points). Our inferred mass fractions come from the recipes in Roediger & Courteau (2015), and the errors from the absolute differences between those and the ones in Bell et al. (2003, HUDF-5's errors are too small to be seen). The solid red lines are the results for local ETGs in C13 simulations, with the dashed lines corresponding to the 16–84 percentile range. The violet data points are individual MGs at $<z>=2$ studied in Szomoru et al. (2012), but we want to emphasize that they are extrapolations as information about their mass profiles is unavailable at these galactocentric distances. The crosses in light violet, light green and golden colours denote the mean values for the $<z>=2$, $<z>=0.65$ and $<z>=0.1$ MG samples, respectively (cf. Fig. 8). There is a rough correlation between galaxy mass and the percentage of mass in the outskirts for the green points, following the simulation predictions. However, it is to note that our data do not follow the local relationship because of the median redshift of our sample ($<z>=0.65$). Most importantly, 5–20 per cent of ETGs stellar mass is located in their 'haloes', above the high-z data points and in stark contrast with recent results for late-type galaxies (Trujillo & Bakos 2013; van Dokkumet al. 2014; Trujillo & Fliri 2016).

5.4 Constraining the merger channel for MG growth

Studies about merger rates always provide an indirect way to look at the assembly history of galaxies, because of the fact that what it is measured is the mass to be accreted as opposed to accreted mass. It is interesting to see whether this could be improved by using very deep images to trace any signature of ongoing merging.

To this end, we have created the following exercise. We take the galaxy light that is not described by the overall galaxy spheroid, i.e. the residuals from subtracting the single Sérsic fit to each galaxy surface brightness profile. Converting those into mass (in an approximate manner, given the information at hand), we can check their relative importance. The reason behind this exercise resides in the fact that some low surface brightness features come from galaxy interactions (at least in HUDF-2, HUDF-3 and HUDF-5). These features are smooth and, as such, very hard to be picked up as potential close pairs. HUDF12 has the potential to detect them at intermediate redshift, opening a new perspective in the mass assembly of MGs.

Nevertheless, we would like to emphasize that this is just a toy model because of fitting a single Sérsic function to deep- and high-resolution images of most ETGs, even in the local universe, leaves residuals that have nothing to do with merging features. This seems to be the case for HUDF-1 and HUDF-2, as their residual images display negative and positive values close to the galaxy centre in perpendicular directions corresponding to the symmetry axes, typical of the presence of a non-subtracted inner galaxy disc (as detected in Section 4.1). Therefore, for these two galaxies, we investigated the residuals coming from the subtraction of a double Sérsic fit instead of a single Sérsic fit.

Table 3. Stellar mass contained in the residuals.

Galaxy	Per cent light in residuals *i* band	Mass $\times 10^8$ M$_\odot$	Per cent galaxy's mass
HUDF-1	0.52 ± 0.06	2.06 ± 0.24	0.79 ± 0.09
HUDF-2	1.03 ± 0.07	10.24 ± 0.71	1.57 ± 0.11
HUDF-3	1.79 ± 0.47	21.47 ± 5.64	2.72 ± 0.71
HUDF-4	0.35 ± 0.10	3.49 ± 0.97	0.54 ± 0.15
HUDF-5	1.41 ± 0.01	33.53 ± 0.31	2.15 ± 0.02
HUDF-6	0.34 ± 0.13	14.15 ± 5.38	0.52 ± 0.20
Mean values	0.91 ± 0.13	14.16 ± 1.69	1.38 ± 0.20

The step to transform from light to mass is done by a crude assumption, i.e. that the mass-to-light ratio is constant through the entire radial distribution. Considering that our galaxy sample have relatively flat colour gradients, this is reasonable. We utilize the value given by the MIUSCAT models[5] (Ricciardelli et al. 2012; Vazdekis et al. 2012) in the reddest (SDSS *i* band) mass-to-light ratio, provided assuming that Kroupa universal IMF, solar metallicity and a stellar population age of 5 Gyr. The results are given in Table 3 and Fig. 11. The errors stem from the different total amount of light enclosed in the *HST* residuals closest to rest-frame *i* band.

[4] http://www.iac.es/proyecto/miles/

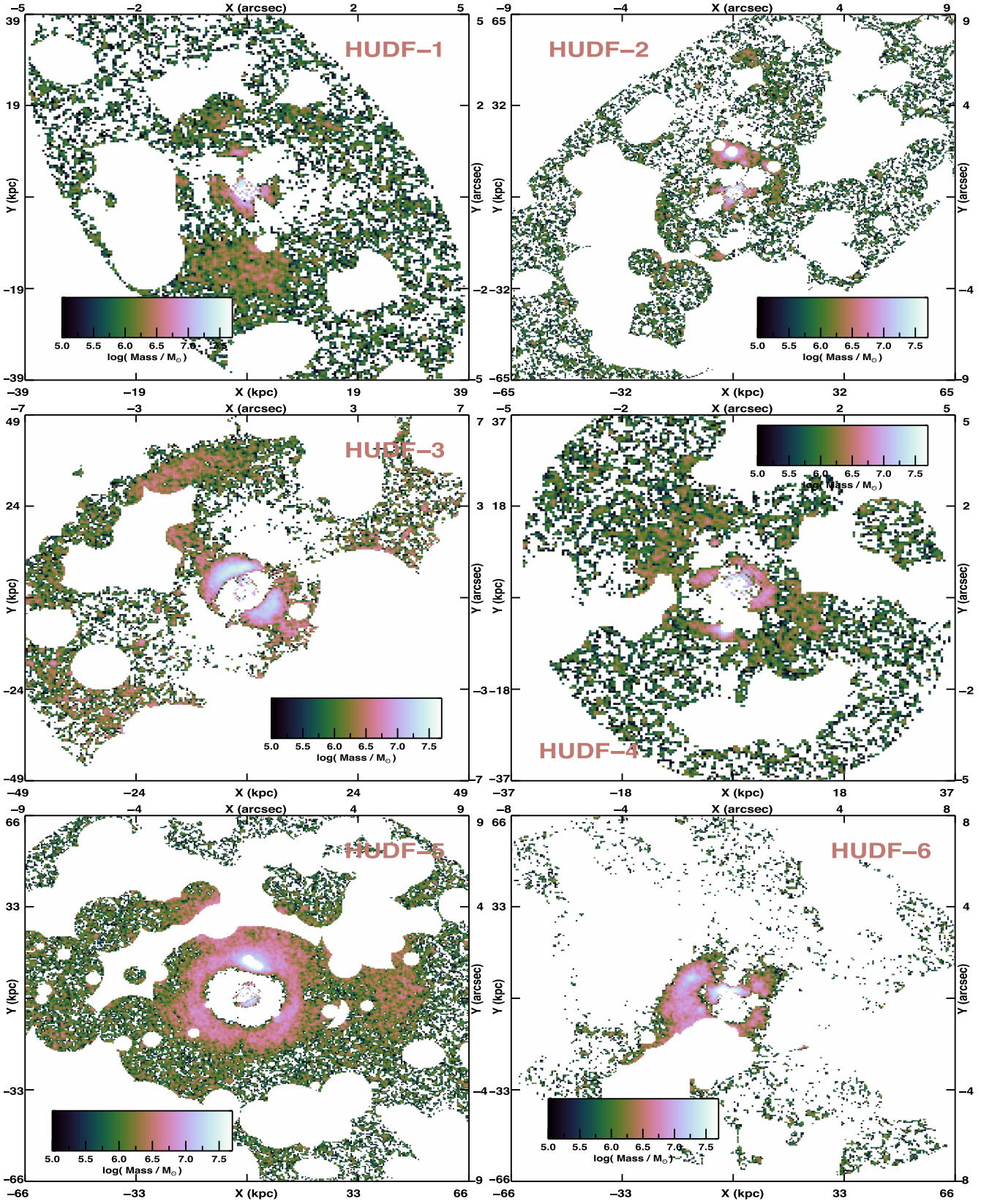

Figure 11. Stellar mass maps corresponding to the smooth residuals in the galaxy light. Thinking of the inside–out growth of MGs, we calculated how much mass is encompassed in minor interactions by subtracting to every galaxy a Sérsic model of its overall spheroid. The colour coding is the same throughout the plots, but each galaxy is shown up to its full extent (31 mag arcsec^{-2}). The white elliptical patches are the product of neighbour masking, and thus the total masses listed in Table 3 for these residuals (1–2 per cent of the total galaxy stellar mass) should be taken as a lower limit. These numbers given by our toy model are not far from the predictions from close pairs to the mass growth of massive ETGs ($\Delta M/M \sim$4 per cent Gyr^{-1}).

Very little light is involved in these smooth features (of the order of 1 per cent the galaxy light), with a slightly larger percentage in mass (1–2 per cent). To put these numbers in context, we compare them with best estimates from satellites/close pairs. Specifically, Ferreras et al. (2014) with a sample of 238 MGs at $0.3 < z < 1.3$ quantified that the upper limit for the average mass growth rate for these galaxies is $(\Delta M/M)/\Delta t \sim 0.08 \pm 0.02$ Gyr^{-1}, while van Dokkum (2005) inferred 0.09 ± 0.04 Gyr^{-1} for 126 red nearby galaxies. To move from growth rate to mass, a time-scale for the duration of the morphological features of dry mergers should be adopted. Bell et al. (2006) classified major (1:1–3:1) merger snapshots, suggesting values of 150 ± 50 Myr. The duration of the visibility of galaxy mergers using CAS parameters is 0.4–1 Gyr (Conselice 2006; Lotz et al. 2008; Conselice, Yang & Bluck 2009). Choosing then 0.5 Gyr as a representative number, one would expect ∼4 per cent of the total mass of the galaxy in these residuals.

Our numbers are close to these expected values, especially by thinking that some residuals in mass are not seen because of our masking. Actually, this aspect makes our measurements a lower bound in the percentages of light and mass. Nevertheless, we believe we cannot draw any strong implications as this experiment has many parameters we do not control: the residuals and the mass-to-light ratios being representative of substructures, the uncertainty about how long merging features last and cosmic variance due to the fact of studying only six MGs. It is to note that the galaxies showing smaller residuals are two most compact ones (HUDF-1 and HUDF-4), and the most distant galaxy (HUDF-6) that might be an indication that cosmological dimming has a deeper impact on it than for the rest of the objects, hiding some extra mass in undetected features. Summarizing, it is very interesting to see that this naive exercise yields numbers similar to close pairs predictions and also to check that the visually identified merging smooth features in HUDF-2, HUDF-3 and HUDF-5 clearly provide to these galaxies with more mass in their residuals.

6 SUMMARY AND CONCLUSIONS

We present a comprehensive characterization of the six most massive ($M_{stellar} \geq 5 \times 10^{10}$ M$_\odot$) ETGs at $z \lesssim 1$ in the deepest *HST* field, the HUDF. We focused our efforts in the HUDF12 programme (Ellis et al. 2013; Koekemoer et al. 2013), whose data reduction preserves extended low surface brightness features and at redshifts where cosmological dimming is not yet strong enough ($\lesssim$2 mag arcsec^{-2}) to remove the traces of minor merging.

The substructures present in the outer parts of ETGs, whose origin is the progressive build-up of these objects via merging, have not been studied to date at intermediate/high redshift due to their intrinsic faintness and the very rapidly growing cosmological dimming, which make these outskirts very challenging to detect. Therefore, it is not yet known whether these outer parts could be described as galactic haloes, similar to those found in disc galaxies. Our work aims to clarify this situation and investigate how MGs change their observational properties since $z = 1$.

We carefully analysed each galaxy image according to the recipes in Trujillo & Bakos (2013), fitting up to four Sérsic functions convolved with the PSF in the eight *HST* filters available. In so doing, we are able to remove the PSF distortion in the observed profiles. Our ultradeep data set reaches galaxy surface brightness profiles down to 31 mag arcsec^{-2} (3σ in 10×10 arcsec boxes; ∼29 mag arcsec^{-2} after correcting by cosmological dimming), which translates into 25 effective radii in distance, or as far as 100 kpc in some cases at an outstanding median redshift of $< z > = 0.65$.

The striking difference between previous shallower observations and the HUDF12 is the appearance of extended low surface brightness envelopes (or stellar haloes) for each individual galaxy. Even though the small statistical representativeness of our sample, containing only six objects, our data set is unique inasmuch as we demonstrate the existence, the relative importance and the spatial distribution of this low surface brightness component for each individual galaxy at study. Of course, longer integration times disclose fainter and fainter features (e.g. Martínez-Delgado et al. 2010; Duc et al. 2015; Trujillo & Fliri 2016), which are key to understanding the assembly history of MGs, although their contribution to the total light and mass decrease in importance. We stress that caution needs to be taken with image data reduction, as indeed the images must be reduced in such a way to preserve low surface brightness features. Providing we work in this direction, the advent of very deep imaging in future years will not only improve our understanding of high-redshift galaxies but will also greatly enhance our comprehension of the nearby Universe.

We placed constraints on the inside–out growth of massive ETGs by estimating their observed surface brightness profiles, equivalent Sloan filters rest-frame profiles and colours, mass profiles and light cumulative fractions. Both *HST* bands and the Sloan filters equivalent photometry show a steady decrease in galaxy flux down to our detection limit without the presence of any truncations. Galaxies displaying signs of merging have surface brightness bumps in their outer parts (at >20 kpc; 25–26 mag arcsec^{-2} rest frame). In general, between 20 and 40 per cent of the light is located at distances beyond 10 kpc. Additionally, when comparing the mean massive ETG mass profiles at different cosmic times, we find that they store a higher fraction of stellar mass in their outer parts (same galactocentric distances) at decreasing redshift, namely 28.7 per cent at $< z > = 0.1$, 15.1 per cent at $< z > = 0.65$ and only 3.5 per cent at $< z > = 2$.

It is very hard to unambiguously define ETG stellar haloes (especially without kinematic information), or even comparing with in situ/accreted material in numerical simulations. However, by integrating both the observational and simulated mass profiles at distances ($10 < R/\mathrm{kpc} < 50$), where hierarchical accretion is dominant over the in situ formed stars, we gather evidence for ETG haloes containing more mass than their late-type counterparts. ETG galaxy stellar haloes host 5–20 per cent of the galaxy mass, in stark contrast with what has been reported for late-type stellar haloes (see fig. 12 in Trujillo & Fliri 2016, only up to 5 per cent). We must emphasize that the median redshift of the six galaxies at study is $< z > = 0.65$, and hence this divergence between early and late types is larger for local Universe massive ETGs. Extended low brightness components are present in all massive ETGs in our sample and they seem to be a ubiquitous ingredient of the ΛCDM paradigm.

Finally, we developed a toy model in order to attempt to determine the total amount of light and mass in smooth features linked with ongoing minor merging interactions. Our parametric fits allow us to model the overall spheroid in each galaxy of our ETG sample. After removing this 2D surface brightness profile, the residual light gives us insight into the ongoing mass assembly as opposed to more indirect methods such as satellite counts. The uncertainties are large, due to the necessary assumptions and the inherent scatter in a galaxy-by-galaxy basis, but the results of this experiment indicate that smooth merging features in our imaging contribute at least 1–2 per cent in galaxy light and mass. The expectation from close pairs is $\Delta M/M \sim 4$ per cent, and our result must be further investigated, but it does not contradict the fact that major and minor mergers seem

to be the dominant mechanisms, driving the evolution of massive ETGs since $z = 1$.

ACKNOWLEDGEMENTS

We warmly thank the anonymous referee for his thorough reading and questions. FB is indebted to James S. Dunlop for his advice, and also for the economic support for MM during her visit to the University of Edinburgh. The IA Thematic Line 'The assembly history of galaxies resolved in space and time' is acknowledged for inviting IT for his visit to the Observatory of Lisbon. We gratefully thank Esther Mármol-Queraltó, Ross McLure, Jesús Falcón-Barroso, Francesco La Barbera, Anton Koekemoer, Hugo Messias and Alexandre Vazdekis for their help through different stages of this project. José Sabater, Britton Smith and Jovan Veljanoski are very much acknowledged for very valuable computational assistance. We have extensively used the following software packages: TOPCAT (Taylor 2005), ALADIN (Bonnarel et al. 2000) and the IDL routines `mpfit` and `mpfitfun` (Markwardt 2009). FB acknowledges the support of the European Research Council via the award of an Advanced Grant to James S. Dunlop, the funding from the ASTRODEEP FP7 programme and the support by FCT via the postdoctoral fellowship SFRH/BPD/103958/2014. This work is supported by Fundação para a Ciência e a Tecnologia (FCT) through national funds (UID/FIS/04434/2013) and by FEDER through COMPETE2020 (POCI-01-0145-FEDER-007672). FB and IT acknowledge support from grant AYA2016-77237-C3-1-P from the Spanish Ministry of Economy and Competitiveness (MINECO). ECL would like to acknowledge financial support from the ERC via an Advanced Grant under grant agreement no. 321323-NEOGAL. APC acknowledges a COFUND/Durham Junior Research Fellowship under EU grant 267209. PGP-G acknowledges support from Spanish Government Grants AYA2012-31277 and AYA2015-70815-ERC. This work has made use of the Rainbow Cosmological Surveys Database, which is operated by the Universidad Complutense de Madrid (UCM), partnered with the University of California Observatories at Santa Cruz (UCO/Lick,UCSC).

REFERENCES

Arnouts S., Cristiani S., Moscardini L., Matarrese S., Lucchin F., Fontana A., Giallongo E., 1999, MNRAS, 310, 540
Atkinson A. M., Abraham R. G., Ferguson A. M. N., 2013, ApJ, 765, 28
Barro G. et al., 2011a, ApJS, 193, 13
Barro G. et al., 2011b, ApJS, 193, 30
Barro G. et al., 2013, ApJ, 765, 104
Beckwith S. V. W. et al., 2006, AJ, 132, 1729
Bell E. F., McIntosh D. H., Katz N., Weinberg M. D., 2003, ApJS, 149, 289
Bell E. F. et al., 2006, ApJ, 640, 241
Bell E. F. et al., 2012, ApJ, 753, 167
Bertin E., Arnouts S., 1996, A&AS, 117, 393
Bezanson R., van Dokkum P. G., Tal T., Marchesini D., Kriek M., Franx M., Coppi P., 2009, ApJ, 697, 1290
Blanton M. R. et al., 2005, AJ, 129, 2562
Bluck A. F. L., Conselice C. J., Buitrago F., Grützbauch R., Hoyos C., Mortlock A., Bauer A. E., 2012, ApJ, 747, 34
Bonnarel F. et al., 2000, A&AS, 143, 33
Bouwens R. J. et al., 2012, ApJ, 752, L5
Boylan-Kolchin M., Springel V., White S. D. M., Jenkins A., Lemson G., 2009, MNRAS, 398, 1150
Bruce V. A. et al., 2012, MNRAS, 427, 1666
Bruzual G., Charlot S., 2003, MNRAS, 344, 1000
Buitrago F., Trujillo I., Conselice C. J., Bouwens R. J., Dickinson M., Yan H., 2008, ApJ, 687, L61
Buitrago F., Trujillo I., Conselice C. J., Häußler B., 2013, MNRAS, 428, 1460
Cassata P. et al., 2010, ApJ, 714, L79
Cassata P. et al., 2011, ApJ, 743, 96
Ceverino D., Dekel A., Tweed D., Primack J., 2015, MNRAS, 447, 3291
Chabrier G., 2003, PASP, 115, 763
Cimatti A. et al., 2008, A&A, 482, 21
Coccato L., Gerhard O., Arnaboldi M., 2010, MNRAS, 407, L26
Cole S., Lacey C. G., Baugh C. M., Frenk C. S., 2000, MNRAS, 319, 168
Conselice C. J., 2006, ApJ, 638, 686
Conselice C. J., Yang C., Bluck A. F. L., 2009, MNRAS, 394, 1956
Cooper A. P., D'Souza R., Kauffmann G., Wang J., Boylan-Kolchin M., Guo Q., Frenk C. S., White S. D. M., 2013, MNRAS, 434, 3348 (C13)
Crnojević D., Ferguson A. M. N., Irwin M. J., Bernard E. J., Arimoto N., Jablonka P., Kobayashi C., 2013, MNRAS, 432, 832
Croom S. M., Smith R. J., Boyle B. J., Shanks T., Loaring N. S., Miller L., Lewis I. J., 2001, MNRAS, 322, L29
Croton D. J. et al., 2006, MNRAS, 365, 11
D'Souza R., Kauffman G., Wang J., Vegetti S., 2014, MNRAS, 443, 1433
Daddi E. et al., 2005, ApJ, 626, 680
Damjanov I. et al., 2009, ApJ, 695, 101
de Jong R. S., 2008, MNRAS, 388, 1521
Duc P. A. et al., 2015, MNRAS, 446, 120
Ellis R. S. et al., 2013, ApJ, 763, L7
Falcón-Barroso J. et al., 2006, New Astron. Rev., 49, 515
Ferré-Mateu A., Vazdekis A., de la Rosa I. G., 2013, MNRAS, 431, 440
Ferreras I. et al., 2014, MNRAS, 444, 906
Fumagalli M. et al., 2014, ApJ, 796, 35
Giavalisco M., Livio M., Bohlin R. C., Macchetto F. D., Stecher T. P., 1996, AJ, 112, 369
Guo Q. et al., 2011, MNRAS, 413, 101
Hopkins P. F., Bundy K., Murray N., Quataert E., Lauer T. R., Ma C. P., 2009, MNRAS, 398, 898
Huang S., Ho L. C., Peng C. Y., Li Z. Y., Barth A. J., 2013, ApJ, 768, L28
Huertas-Company M. et al., 2013, MNRAS, 428, 1715
Ilbert O. et al., 2006, A&A, 457, 841
Kaviraj S., 2010, MNRAS, 406, 382
Khochfar S., Silk J., 2006, ApJ, 648, L21
Koekemoer A. M. et al., 2013, ApJS, 209, 3
Kormendy J., Fisher D. B., Cornell M. E., Bender R., 2009, ApJS, 182, 216
Krajnović D. et al., 2008, MNRAS, 390, 93
Krajnović D. et al., 2013, MNRAS, 432, 1768
Krist J., 1995, in Shaw R. A., Payne H. E., Hayes J. J. E., eds, ASP Conf. Ser. Vol. 77, Astronomical Data Analysis Software and Systems IV. Astron. Soc. Pac., San Francisco, p. 349
La Barbera F., Ferreras I., de Carvalho R. R., Bruzual G., Charlot S., Pasquali A., Merlin E., 2012, MNRAS, 426, 2300
La Barbera F., Ferreras I., Vazdekis A., de la Rosa I. G., de Carvalho R. R., Trevisan M., Falcón-Barroso J., Ricciardelli E., 2013, MNRAS, 433, 3017
Le Fèvre O. et al., 2005, A&A, 439, 845
López-Sanjuan C. et al., 2012, A&A, 548, A7
Lotz J. M., Jonsson P., Cox T. J., Primack J. R., 2008, MNRAS, 391, 1137
McLure R. J. et al., 2013, MNRAS, 432, 2696
Markwardt C. B., 2009, in Bohlender D. A., Durand D., Dowler P., eds, ASP Conf. Ser. Vol. 411, Astronomical Data Analysis Software and Systems XVIII. Astron. Soc. Pac., San Francisco, p. 251
Mármol-Queraltó E., Trujillo I., Pérez-González P. G., Varela J., Barro G., 2012, MNRAS, 422, 2187
Mármol-Queraltó E., Trujillo I., Villar V., Barro G., Pérez-González P. G., 2013, MNRAS, 429, 792
Martín-Navarro I. et al., 2015, ApJ, 798, L4
Martínez-Delgado D. et al., 2010, AJ, 140, 962
Newman A. B., Ellis R. S., Bundy K., Treu T., 2012, ApJ, 746, 162
Oke J. B., Gunn J. E., 1983, ApJ, 266, 713
Oser L., Ostriker J. P., Naab T., Johansson P. H., Burkert A., 2010, ApJ, 725, 2312

Peng C. Y., Ho L. C., Impey C. D., Rix H. W., 2010, AJ, 139, 2097
Pérez-González P. G. et al., 2008a, ApJ, 675, 234
Pérez-González P. G., Trujillo I., Barro G., Gallego J., Zamorano J., Conselice C. J., 2008b, ApJ, 687, 50
Pirzkal N. et al., 2005, ApJ, 622, 319
Purcell C. W., Bullock J. S., Zentner A. R., 2007, ApJ, 666, 20
Ravikumar C. D. et al., 2007, A&A, 465, 1099
Rejkuba M., Harris W. E., Greggio L., Harris G. L. H., Jerjen H., Gonzalez O. A., 2014, ApJ, 791, L2
Ribeiro B. et al., 2016, A&A, 593, A22
Ricciardelli E., Trujillo I., Buitrago F., Conselice C. J., 2010, MNRAS, 406, 230
Ricciardelli E., Vazdekis A., Cenarro A. J., Falcón-Barroso J., 2012, MNRAS, 424, 172
Roediger J. C., Courteau S., 2015, MNRAS, 452, 3209
Ruiz P., Trujillo I., Mármol-Queraltó E., 2015, MNRAS, 454, 1605
Salpeter E. E., 1955, ApJ, 121, 161
Sandin C., 2014, A&A, 567, A97
Sandin C., 2015, A&A, 577, A106
Szomoru D., Franx M., van Dokkum P. G., 2012, ApJ, 749, 121
Tal T., van Dokkum P. G., 2011, ApJ, 731, 89
Tal T., van Dokkum P. G., Nelan J., Bezanson R., 2009, AJ, 138, 1417
Taylor M. B., 2005, in Shopbell P., Britton M., Ebert R., eds, ASP Conf. Ser. Vol. 347, Astronomical Data Analysis Software and Systems XIV. Astron. Soc. Pac., San Francisco, p. 29
Toft S. et al., 2007, ApJ, 671, 285
Trujillo I., Bakos J., 2013, MNRAS, 431, 1121
Trujillo I., Fliri J., 2016, ApJ, 823, 123
Trujillo I. et al., 2006a, MNRAS, 373, L36
Trujillo I. et al., 2006b, ApJ, 650, 18
Trujillo I., Conselice C. J., Bundy K., Cooper M. C., Eisenhardt P., Ellis R. S., 2007, MNRAS, 382, 109
Trujillo I., Ferreras I., de La Rosa I. G., 2011, MNRAS, 415, 3903
Trujillo I., Ferré-Mateu A., Balcells M., Vazdekis A., Sánchez-Blázquez P., 2014, ApJ, 780, L20
van der Wel A. et al., 2014, ApJ, 788, 28
van Dokkum P. G., 2005, AJ, 130, 2647
van Dokkum P. G. et al., 2010, ApJ, 709, 1018
van Dokkum P. G., Abraham R., Merritt A., 2014, ApJ, 782, L24
Vanzella E. et al., 2005, A&A, 434, 53
Vazdekis A., Ricciardelli E., Cenarro A. J., Rivero-González J. G., Díaz-García L. A., Falcón-Barroso J., 2012, MNRAS, 424, 157
Wellons S. et al., 2016, MNRAS, 456, 1030
Williams C. C. et al., 2014, ApJ, 780, 1
Xie L., Guo Q., Cooper A. P., Frenk C. S., Li R., Gao L., 2015, MNRAS, 447, 636
Zackrisson E., Bergvall N., Östlin G., Micheva G., Leksell M., 2006, ApJ, 650, 812
Zibetti S., Ferguson A. M. N., 2004, MNRAS, 352, L6
Zibetti S., White S. D. M., Brinkmann J., 2004, MNRAS, 347, 556
Zolotov A. et al., 2015, MNRAS, 450, 2327

APPENDIX A: *H*-BAND PROFILES

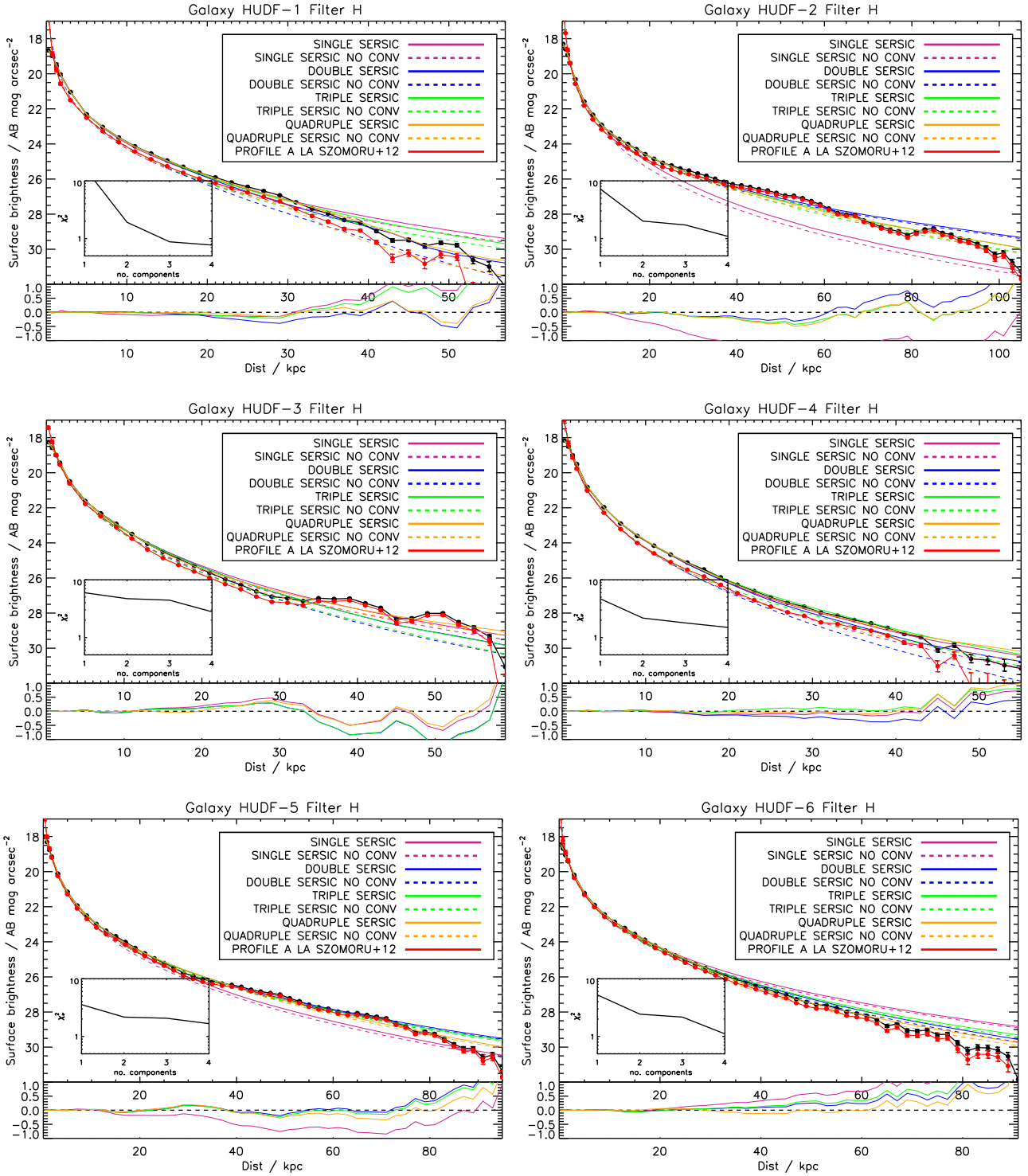

Figure A1. Observed (black line), model (convolved and non-convolved with the PSF, coloured solid and dashed lines, respectively, with colours indicated in the legend) and 'a la Szomoru' (deconvolved adding the residuals of the four Sérsic fit; red line) galaxy surface brightness profiles for our galaxy sample in the *H* band. The subplot shows the reduced chi-square (χ^2_ν) values for the Sérsic fits we performed. The bottom miniplots display the differences between the observed surface brightness profile and the multi-Sérsic PSF convolved models.

This paper has been typeset from a TEX/LATEX file prepared by the author.